

# Magnetosheath compression: Role of characteristic compression time, alpha particle abundance and alpha/proton relative velocity

Petr Hellinger and Pavel Trávníček

Institute of Atmospheric Physics, AS CR, Prague, Czech Republic

## Abstract.

Hybrid expanding box (HEB) is used to study a slow compression of the magnetosheath plasma. The HEB simulations confirm the previous results of *Hellinger et al.* [2003b]: the slowly compressed plasma follows a marginal stability path of the proton cyclotron instability in a low-beta plasma whereas in a high-beta plasma the mirror instability becomes dominant. For a faster compression the marginal stability path shifts further inside the unstable region in order to balance the faster anisotropization rate due to the faster compression. The presence of alpha particles strongly changes the dispersive properties of the plasma and introduces the alpha cyclotron instability. The theoretical description of the system becomes intricate since the alpha particles introduce additional parameters. The plasma evolution during the compression gets more complex; a transition between the proton and the alpha cyclotron instabilities appears. The overall behavior of the simulated system is not qualitatively different from the behavior of the pure electron-proton plasma. When an additional parameter, a nonzero alpha/proton relative velocity is included the theoretical understanding becomes even more complicated. The behavior of the compressed system is nevertheless similar to the results in the pure electron-proton plasma. An important qualitative change from the zero alpha/proton relative velocity case is that the proton cyclotron instability is able to efficiently accelerate alpha particles with respect to protons whereas the alpha cyclotron and the mirror instabilities decelerate them.

## 1. Introduction

Properties of collisionless plasmas are largely determined by wave-particle interactions. A well-known example of such wave-particle interaction is the Earth's magnetosheath: The magnetosheath plasma flow around the magnetospheric cavity exhibits large-scale inhomogeneities [*Phan et al.*, 1994; *Hill et al.*, 1995]. These large-scale processes locally translate for example as compression, expansion or velocity shear and induce a particle temperature anisotropy, a difference between the perpendicular temperature  $T_{\perp}$  and the parallel temperature  $T_{\parallel}$  (perpendicular and parallel denotes directions with respect to the ambient magnetic field).  $T_{\perp} > T_{\parallel}$  is typically observed in the day-side magnetosheath [*Anderson and Fuselier*, 1993] whereas  $T_{\perp} < T_{\parallel}$  is often observed in the night-side magnetosheath [*Matsuoka et al.*, 2002]. The day-side magnetosheath behind the quasi-perpendicular portion of the Earth's bow shock is dominated by locally generated waves [*Lacombe and Belmont*, 1995; *Schwartz et al.*, 1996; *Hubert et al.*, 1998]: Transverse Alfvén ion cyclotron waves are observed in low-beta regions whereas compressional mirror waves are observed in high-beta regions. These waves are generated by ion temperature anisotropies  $T_{\perp} > T_{\parallel}$ , and are usually observed near the marginal stability of the corresponding instability [*Anderson and Fuselier*, 1993]. As a consequence, the magnetosheath protons are characterized by an anticorrelation [*Fuselier et al.*, 1994; *Gary et al.*, 1994c] between the proton temperature anisotropy  $A_p = T_{p\perp}/T_{p\parallel}$  and the proton parallel beta  $\beta_{p\parallel}$

$$A_p - 1 \sim \frac{a}{\beta_{p\parallel}^b}$$

where  $a \sim 1$  and  $b \sim 0.5$ . This anticorrelation is consistent with the marginal stability relation of these instabilities: their

linear growth rate is close to the threshold  $\gamma \sim 0$ . A similar anticorrelation between the alpha particle temperature anisotropy  $A_{\alpha} = T_{\alpha\perp}/T_{\alpha\parallel}$  and the alpha particle parallel beta  $\beta_{\alpha\parallel}$  is also sometimes observed. These observations suggest that the magnetosheath plasma follows a marginal stability path [*Manheimer and Boris*, 1977] in the space  $(\beta_{p\parallel}, A_p)$ . Results of kinetic simulation studies [e.g. *McKean et al.*, 1994] support the hypothesis of the marginal stability path based on the observations. This path could be approximatively traced by a set of standard simulations varying the initial plasma parameters. The observations and kinetic numerical simulations led to the development of a bounded anisotropy model [*Gary et al.*, 1994a; *Denton et al.*, 1994] as a suitable closure of the magnetohydrodynamic models [e.g. *Erkaev et al.*, 2000; *Pudovkin et al.*, 2002b].

Recently, *Hellinger et al.* [2003b] used a hybrid expanding box (HEB) model [*Liewer et al.*, 2001; *Hellinger et al.*, 2003a] to study an influence of a slow compression (i.e. when the characteristic compression time is much greater than the ion gyroperiod) on the plasma properties. The HEB simulation showed in a direct and comprehensive way that the plasma follows the marginal stability path. This path in the case of the slow compression goes from the low-beta to the high-beta plasma and is characterized by a growth of fluctuating wave energy. The results of *Hellinger et al.* [2003b] are not generally applicable in the context of the magnetosheath (and especially in the context of the depletion layer, the subsolar region between the magnetosheath and the magnetopause). The magnetosheath flow induces a combination of compression and expansion (field-line stretching) and for example the depletion layer [cf. e.g. *Farrugia et al.*, 2001], is characterized by an anticorrelation between the magnitude of the magnetic field (which increases when approaching magnetopause) and the plasma density (which decreases at the same time). These properties indicate a presence of the field-line stretching and the compression in a direction highly oblique with respect to the ambient magnetic field (see Equations (3) and (4)). In this region  $\beta_{p\parallel}$  decreases when approaching the magnetopause and  $A_p$  increases. The fluctuating wave amplitude (in low-beta regions there are mainly ion cyclotron waves)

is correlated with  $\beta_{p\parallel}$  [Gary *et al.*, 1993a; Anderson *et al.*, 1994] and therefore decreases as well. However, the presence of the depletion layer near the magnetopause is not a general feature. In situ observations of [Lucek *et al.*, 1999] show that the flank regions near the magnetopause are sometimes characterized by a strong mirror turbulence. The strong mirror turbulence near the magnetopause is not compatible with the usual low-beta condition of the depletion region and may be a consequence of the plasma compression as a dominant process.

In this paper we extend the work of Hellinger *et al.* [2003b] on the plasma compression using the HEB code. We start with a short description of the code in section 2. In section 3 we give theoretical predictions for the behavior of the simulated system, CGL and linear kinetic theory. We present the simulation results in the section 4 and compare them with theoretical predictions: The first physical problem we study is an influence of the characteristic compression time on the plasma evolution in section 4.1. We perform three simulations with different characteristic compression times and investigate how the marginal stability path depends on the characteristic time.

The second problem we study is the role of alpha particles and we present the results in the section 4.2. Alpha particles have typically abundances around few percents of electron number density [Bame *et al.*, 1975]. Their presence changes the dispersion properties: The dispersion involves two distinct cyclotron branches and two corresponding instabilities: the proton and alpha cyclotron instabilities. Both instabilities may be dominant depending on plasma parameters. The alpha cyclotron instability dominates over the proton one, for example, in a high beta plasma and/or for a high abundance of alpha particles [Gary *et al.*, 1994b]. We study the relationship between the two instabilities and the mirror one.

Properties of the magnetosheath plasma containing electrons, protons and alpha particles are usually studied under assumption that there is no relative velocity between protons and alpha particles. On the other hand, in situ observations in the fast solar wind [Marsch *et al.*, 1982; Neugebauer *et al.*, 1996; Reisenfeld *et al.*, 2001] show that alpha particles are typically faster than protons and that the alpha/proton velocity  $v_{\alpha p}$  (henceforth we will use “alpha/proton velocity” as a short-hand for “relative magnetic-field-aligned velocity between the two species”) is comparable with the local Alfvén velocity. The non zero alpha/proton velocity typically observed in the fast solar wind, may also persist and be further enhanced during the crossing of a shock: Peterson *et al.* [1979] proposed a model which predicts that the alpha particles are decelerated less than protons by the cross-shock potential [cf. Zhao *et al.*, 1991; Gratton and Farrugia, 1996]. In situ observations by Ogilvie *et al.* [1982] and Fuselier *et al.* [1988] support this behavior of alpha particles during the shock crossing.

The evolution of the alpha/proton velocity in the magnetosheath and in the depletion layer is not well known. The properties of the plasma with the alpha/proton velocity has been studied in the context of the solar wind [e.g. Gomberoff *et al.*, 1996; Li and Habbal, 2000; Gary *et al.*, 2003, and references therein]: the alpha/proton velocity changes dispersion relations and resonance conditions of different branches and introduces different properties of the wave propagating along and against the alpha/proton velocity. However, an understanding of the system with the alpha/proton velocity is by no means complete owing to many plasma parameters involved. Gary *et al.* [2003] studied a relation between the alpha/proton velocity and the proton and alpha cyclotron instabilities. Both instabilities remove the ion temperature anisotropies and moreover change the alpha/proton velocity. In agreement with the quasi-linear expectations, the alpha cyclotron instability decelerates the alpha particles [Gary *et al.*, 2003, Figures 1 and 3] whereas the proton cyclotron instability accelerated them, at least during the initial linear/quasi-linear phase [Gary *et al.*, 2003, Figure 5]; the alpha particles were decelerated later on in these simulations. The deceleration was stronger in higher beta plasmas. The physical mechanism of the deceleration was, however, not elucidated by Gary *et al.* [2003].

The results of Gary *et al.* [2003] indicate that the alpha particles may be accelerated or decelerated in the magnetosheath. It

is an open question whether the non zero alpha/proton velocity may persist further in the magnetosheath and in the depletion layer. The theoretical investigations by Gratton and Farrugia [1996] and Gnani *et al.* [2000] suggest that there exists an alpha/proton velocity in the depletion layer. Gratton and Farrugia [1996] and Gnani *et al.* [2000] studied the linear properties of ion cyclotron waves and showed that some of their spectral properties observed in the depletion layer may be explained by a presence of a non negligible alpha/proton velocity.

These theoretical, observation and simulation results led us to investigate in section 4.3 an influence of the alpha/proton velocity on plasma properties and instabilities during the compression in the magnetosheath (and solar wind) context. The simulation results of different problems are summarized and discussed in the section 5. We conclude the paper by section 6 followed by Appendix describing our simulation model in detail.

## 2. Hybrid expanding box model

In this paper we use a modified version of a two-dimensional (2-D) hybrid code [Matthews, 1994; Hellinger *et al.*, 2003a], the HEB code. The HEB code was developed in the context of the expanding solar wind and Hellinger *et al.* [2003b] applied this model in the magnetosheath context. The physical motivation behind the HEB code is the assumption that the typical scales of macroscopic processes as expansion and compression are usually much larger than the kinetic ion (and electron) scales. In this approximation the plasma may be considered locally as a homogeneous medium with flow-induced processes; the flow velocity  $\mathbf{U} = \mathbf{U}(\mathbf{x})$  is characterized by the stress tensor  $\mathbf{T}$

$$T_{ij} = \frac{\partial U_i}{\partial x_j}. \quad (1)$$

Assume that the asymmetric part of the stress tensor  $\mathbf{T}$  is negligible (i.e. neglecting the velocity shear) and that the tensor  $\mathbf{T}$  has three eigenvalues  $\lambda_{1,2,3}$  and three corresponding orthogonal eigenvectors  $\mathbf{w}_{1,2,3}$ . The positive eigenvalues  $\lambda_i$  correspond to the expansion whereas the negative eigenvalues  $\lambda_i$  correspond to the compression. If we assume that gradients are small so that the stress tensor  $\mathbf{T}$  is about constant along the stream lines a small volume of plasma in the direction of the eigenvector  $\mathbf{w}_i$  changes as

$$L_i(t) = 1 + \lambda_i t \quad (2)$$

along the eigenvectors  $\mathbf{w}_i$ . Then the plasma density evolves as

$$n(t) = \frac{n(0)}{L_1(t)L_2(t)L_3(t)} \quad (3)$$

whereas the magnetic field evolves as

$$\mathbf{B}(t) = \frac{\sum_i L_i(t)(\mathbf{B}(0) \cdot \mathbf{w}_i)\mathbf{w}_i}{L_1(t)L_2(t)L_3(t)}. \quad (4)$$

Parallel and perpendicular temperatures according the CGL prediction evolve differently

$$T_{\perp} \propto \frac{1}{|\mathbf{B}|}, \quad T_{\parallel} \propto \frac{n^2}{|\mathbf{B}|^2}. \quad (5)$$

which leads to the appearance of the ion temperature anisotropy and the corresponding instabilities. The plasma properties depend on the flow geometry, the expansion along the ambient magnetic field  $\mathbf{B}$  (the field-line stretching) and the compression in a direction perpendicular to  $\mathbf{B}$  lead to  $T_{\perp} > T_{\parallel}$  whereas an expansion perpendicular to  $\mathbf{B}$  and compression along  $\mathbf{B}$  lead to  $T_{\perp} < T_{\parallel}$ .

In the present paper we model the compression as being perpendicular to the ambient magnetic field  $B = (B_0, 0, 0)$ . The direction is chosen to be in  $y$  direction (i.e. is included in the 2-D simulation box). The simulation-box coordinates are co-moving with the plasma, the physical lengths  $x_r$  evolve as  $x_r = \mathbf{L} \cdot \mathbf{x}$  where  $\mathbf{L}$  is a diagonal matrix  $\mathbf{L} = \text{diag}(L_1, L_2, L_3)$  with  $L_1 = L_3 = 1$ , and  $L_2 = 1 - t/t_c$ , where  $t_c$  is a characteristic time of the compression. Note that the compression is imposed in only one direction [cf. *Hellinger et al.*, 2003b] which is appropriate for the magnetosheath context (i.e. we suppose the direction of compression is along the magnetopause normal direction). The model solves the evolution of the system in the coordinates  $\xi$  and  $\nu$  co-moving with the compression. For a more detailed description of the code we refer the reader to the Appendix.

The characteristic spatial and temporal units used in the model are  $c/\omega_{pp0}$  and  $1/\omega_{cp0}$  respectively, where  $c$  is the speed of light,  $\omega_{pp0} = (n_0 e^2 / m_p \epsilon_0)^{1/2}$  is the initial proton plasma frequency, and  $\omega_{cp0} = eB_0 / m_p$  is the initial proton gyrofrequency ( $B_0$  is the initial magnitude of the ambient magnetic field  $\mathbf{B}_0$ ,  $n_0$  is the initial density,  $e$  and  $m_p$  are the proton electric charge and mass, respectively; finally,  $\epsilon_0$  is the dielectric permittivity of vacuum). We use the spatial resolution  $\Delta x = 0.25$  and  $\Delta y = 1$ , and there are 256 particles per cell for each ion specie. Fields and moments are defined on a 2-D grid with dimensions  $512 \times 256$ . The time step for the particle advance is  $\Delta t = 0.02/\omega_{p0}$ , while the magnetic field  $\mathbf{B}$  is advanced with a smaller time step  $\Delta t_B = \Delta t/10$ . The initial ambient magnetic field is  $\mathbf{B}_0 = (B_0, 0, 0)$  and the continuous compression in  $y$  direction leads to an increase of the density and the magnitude of the magnetic field

$$n, B \propto \frac{1}{1 - \frac{t}{t_c}}. \quad (6)$$

The simulation box becomes singular at  $t = t_c$ , therefore we present the simulation results which are not affected by this singularity.

### 3. CGL and linear theory predictions

In the case of a slow compression one expects that the first and the second adiabatic invariants will be conserved [*Chew et al.*, 1956]: HEB simulations [*Hellinger et al.*, 2003a, b] show such an ideal evolution as long as a wave activity in the simulations is negligible. Nonideal effects (as a heat flux and a wave activity) are expected break the invariants in the magnetosheath and lead to a different behavior [*Belmont and Mazelle*, 1992; *Hau*, 1996]; one possibility is an evolution controlled by an instability [*Manheimer and Boris*, 1977]. In this section we briefly outline the CGL and linear theory for sake of comparison with the simulation results in the next section.

The CGL prediction of particle temperature anisotropy and parallel beta in the expanding box reads from Equations (5) and (6) as

$$\frac{T_{\perp}}{T_{\parallel}} \propto \frac{1}{1 - \frac{t}{t_c}}, \quad \beta_{\parallel} \propto 1 - \frac{t}{t_c}. \quad (7)$$

The temperature anisotropy  $T_{\perp}/T_{\parallel}$  increases with time. When the anisotropy exceeds a certain threshold then the cyclotron and mirror instabilities appear. In this paper we mainly focus our interest to the low-beta plasma where the proton and alpha cyclotron instabilities dominate. These instabilities have maximum growth rate at the parallel propagation with respect to the ambient magnetic field. The dispersion relation for left-handed, parallel electromagnetic waves in a homogeneous plasma which consists of bi-Maxwellian particles with a magnetic-field-aligned velocities may be written as [e.g. *Stix*, 1992]:

$$1 - \frac{c^2 k^2}{\omega^2} + \sum_s \frac{\omega_{ps}^2}{\omega^2} \{A_s - 1 + A_s \zeta_s Z(\xi_s)\} = 0, \quad (8)$$

where

$$\xi_s = \frac{\omega - kv_{s\parallel} - \omega_{cs}}{\sqrt{2}kv_{th\parallel s}}, \quad \zeta_s = \frac{\omega - kv_{s\parallel} - (1 - 1/A_s)\omega_{cs}}{\sqrt{2}kv_{th\parallel s}},$$

and  $A_s$  is the temperature anisotropy,  $A_s = T_{s\perp}/T_{s\parallel}$ . In these expressions  $s$  denotes a specie ( $p$  stands for protons,  $e$  for electrons  $e$ , and  $\alpha$  for alpha particles),  $\omega_{cs}$  and  $\omega_{ps}$  denote cyclotron and plasma frequency of the specie  $s$ , respectively,  $v_{s\parallel}$  and  $v_{th\parallel s}$  denote the mean parallel and the thermal velocity of the specie  $s$ , respectively.

### 4. Simulation results

We perform 7 simulations with few different initial parameters, namely the characteristic compression time  $t_c$ , the abundance of alpha particles  $n_{\alpha}/n_e$ , alpha-particle parallel beta  $\beta_{\alpha\parallel 0}$ , and finally the alpha/proton velocity  $v_{\alpha p 0}$ . Table 1 provides an overview of the initial parameters for the simulations we study in the next four subsections for further references.

**Table 1.** Initial parameters of the HEB simulations

Run	$\beta_{p\parallel 0}$	$A_{p0}$	$n_{\alpha}/n_e$	$v_{\alpha p 0}$	$\beta_{\alpha\parallel 0}$	$A_{\alpha 0}$	$t_c$
1	0.1	1.5	0				1000
2	0.1	1.5	0				2000
3	0.1	1.5	0				4000
4	0.1	1.5	5%	0	0.005	1.5	2000
5	0.1	1.5	10%	0	0.01	1.5	2000
6	0.1	1.5	5%	0.5	0.005	1.5	2000
7	0.1	1.5	5%	1	0.005	1.5	2000

#### 4.1. Role of characteristic compression time

Let us start with the description of simulation results for the plasma composed only of protons and electrons. We perform three simulations: Runs 1, 2, and 3 with the characteristic times  $t_c = 1000, 2000,$  and  $4000$ , respectively (see Table 1). All these simulations start with the same initial plasma conditions,  $\beta_{p\parallel 0} = 0.1$  and  $A_{p0} = 1.5$ . The plasma is initially homogeneous and stable with respect to the proton cyclotron instability as well as to the mirror one.

The evolution of plasma properties during the compression for the three simulations is shown in Figure 1. Figure 1 displays the evolution in the space  $(\beta_{p\parallel}, A_p)$  for the Runs 1 ( $t_c = 1000$ , dashed curve), 2 ( $t_c = 2000$ , solid curve), and 3 ( $4000$ , dash-dotted curve). In order to compare simulation results with the linear theory we have investigated the growth rate  $\gamma$  of the proton cyclotron instability in a homogeneous plasma which consists of isotropic electrons and of anisotropic bi-Maxwellian protons using Equation (8). We have calculated the dispersion  $\omega = \omega(k)$  for wave vectors in the interval  $0.01 \leq k \leq 2.5$  for a set of proton parameters:  $0.01 \leq \beta_{p\parallel} \leq 30$  and  $0.1 \leq A_p - 1 \leq 10$ . The electrons and the protons have  $v_{e\parallel} = v_{p\parallel} = 0$  and the electron beta is  $\beta_e = 0.1$ . For each  $\beta_{p\parallel}$  and  $A_p$  we have calculated the maximum growth rate  $\gamma_{PC}$  in the interval  $0.01 \leq k \leq 2.5$ . The result of this calculation,  $\gamma_{PC} = \gamma_{PC}(\beta_{p\parallel}, A_p)$  is shown in Figure 1 as a gray-scale plot: Darker gray denotes stronger instability whereas white corresponds to stable or marginally stable region.

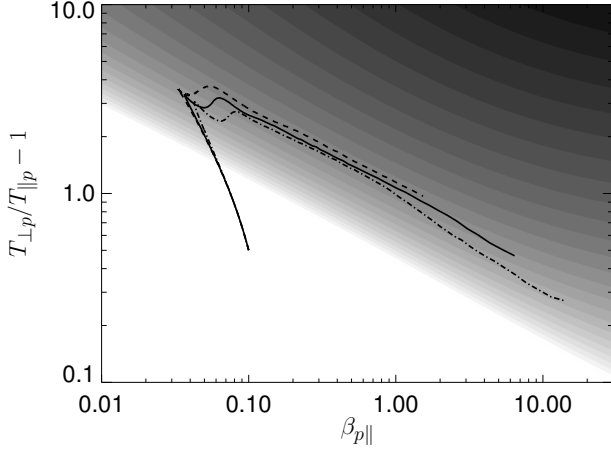


**Figure 1.** Evolution during the plasma compression in the space  $(\beta_{p\parallel}, A_p)$  for Runs 1 ( $t_c = 1000$ , dashed curve), 2 ( $t_c = 2000$ , solid curve), and 3 ( $t_c = 4000$ , dash-dotted curve); see Table 1. The gray-scale plot denotes the linear prediction of maximum growth rate  $\gamma_{PC} = \gamma_{PC}(\beta_{p\parallel}, A_p)$  of the proton cyclotron instability: Darker gray denotes stronger instability whereas white corresponds to stable or marginally stable regions.

In agreement with the previous simulation results [Hellinger *et al.*, 2003b] the evolution of the compressed plasma in the three simulations may be split into three phases. During the first phase, the plasma is stable with respect to the proton cyclotron and mirror instabilities, and it evolves double-adiabatically in agreement with Equation (7). This adiabatic evolution translates into an upward motion in the space  $(\beta_{p\parallel}, A_p)$  of Figure 1. This evolution leads to the development of an important proton temperature anisotropy. The second phase starts when the anisotropy becomes stronger than the threshold for the proton cyclotron instability. During this phase the generated waves heat the plasma and the evolution departs from the double adiabaticity. After a short transition the evolution in the three simulations is similar and follows a constant value of the maximum linear growth rate  $\gamma_{PC}$

$$\gamma_{PC} \sim \gamma_{\text{marg}} = \begin{cases} 0.060 & \text{for } t_c = 1000 \\ 0.050 & \text{for } t_c = 2000 \\ 0.045 & \text{for } t_c = 4000. \end{cases} \quad (9)$$

The system remains near the marginal stability and for a stronger compression (a smaller  $t_c$ ) the system goes further to the unstable region. The parameter  $\gamma_{\text{marg}}$  seems to be inversely proportional to  $t_c$ :

$$\gamma_{\text{marg}} \propto \frac{1}{t_c}. \quad (10)$$

The second phase represents an example of the evolution along the marginal stability path with respect to the proton cyclotron instability.

The third phase is clearly seen in Run 3 and less clearly in Runs 1 and 2. Run 1 becomes influenced by the singularity around  $\beta_{p\parallel} \sim 1$  so that the third phase is not clearly evident. This third phase is characterized by a departure from the relation  $\gamma_{PC} \sim \gamma_{\text{marg}} = \text{const.}$  The transition takes place in the region  $\beta_{p\parallel} \sim 1$  and appears sooner for Run 3 than for Run 2. The transi-

tion exists owing to the development of the mirror instability which becomes important in the high-beta plasma (see below).

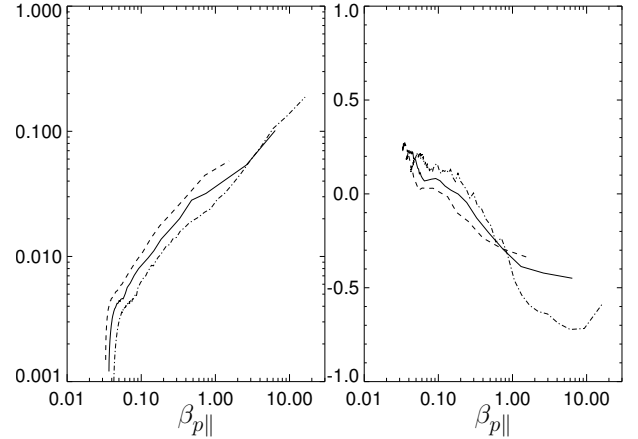


**Figure 2.** (left) The total fluctuating wave energy  $|\delta B|^2/B_0^2$ , and (right) the correlation between  $\delta B_{\parallel}$  and  $n_p$  as a function of  $\beta_{p\parallel}$  for Runs 1 ( $t_c = 1000$ , dashed curves), 2 ( $t_c = 2000$ , solid curves), and 3 ( $t_c = 4000$ , dash-dotted curves).

During the second and the third phases the fluctuating wave energy increases as documented in Figure 2 [cf. Figure 2 of Hellinger *et al.*, 2003b]. Figure 2 shows (left) the evolution of the relative intensity of magnetic field oscillations  $|\delta B|^2/B^2$  and (right) the correlation between the parallel component of magnetic field  $\delta B_{\parallel}$  and the proton density  $n_p$  as a function of  $\beta_{p\parallel}$  for Runs 1 ( $t_c = 1000$ , dashed curve), 2 ( $t_c = 2000$ , solid curve), and 3 ( $t_c = 4000$ , dash-dotted curve). The intensity of the magnetic fluctuations increases with  $\beta_{p\parallel}$  for the three simulations. For a given  $\beta_{p\parallel}$  the intensity is stronger for a faster compression (a smaller  $t_c$ ):

$$\frac{|\delta B|^2}{B^2} \propto \frac{1}{t_c}. \quad (11)$$

Equation (11) is compatible with Equation (10) and may be interpreted as a reaction of the plasma to the compression: In order to balance a faster compression (which anisotropize the protons faster) a stronger wave amplitude is needed to guarantee a faster scattering/isotropization [cf. Gary *et al.*, 2000]. Equation (11) becomes invalid in the high-beta plasma where  $|\delta B|^2/B^2$  is similar for Runs 2 and 3. In the region  $\beta_{p\parallel} \gtrsim 1$  the correlation  $\langle \delta B_{\parallel}, n_p \rangle$  gets negative which is a clear indication of the mirror mode that becomes important in the high-beta plasma. The development of the mirror mode disrupts the second phase and causes the departure from the constant  $\gamma_{PC}$  evolution, Equation (9). This effect was described and discussed in Hellinger *et al.* [2003b]. The different behavior of the proton cyclotron instability and the mirror one and their competition may be responsible for the similar  $|\delta B|^2/B^2$  in Runs 2 and 3. It is also possible that Run 2 is influenced by the approach of the singularity. Let us now move on and study the role of alpha particles.

#### 4.2. Role of Alpha Particles

The presence of alpha particles changes the plasma properties. Instead of one instability there are two of them: the proton cyclotron instability and the alpha cyclotron one. In order to investigate the two cyclotron instabilities and a relation between them (and the impact of the mirror instability) we perform two simulations for  $t_c = 2000$ : Run 4 with  $n_{\alpha}/n_e = 5\%$  and  $\beta_{\alpha\parallel} = 0.05$  and Run 5 with  $n_{\alpha}/n_e = 10\%$  and  $\beta_{\alpha\parallel} = 0.1$ . Runs 4 and 5 start with the same initial conditions for protons as were used in the previous section 4.1 (see Table 1). Moreover for alpha particles we

set the temperature anisotropy to  $A_{\alpha 0} = A_{p0} = 1.5$ . The chosen initial states of Runs 4 and 5 are stable with respect to the proton and alpha cyclotron, and mirror instabilities.

The evolutions of protons and alpha particles during the compression for Runs 4 and 5 are shown in Figure 3: Left panel of Figure 3 displays the evolution in the space  $(\beta_{p\parallel}, A_p)$  whereas right panel of Figure 3 displays the evolution in the space  $(\beta_{\alpha\parallel}, A_\alpha)$  for Runs 4 ( $n_\alpha/n_e = 5\%$ , solid curve) and 5 ( $n_\alpha/n_e = 10\%$ , dashed curve); see Table 1.

As in the previous section we have investigated the stability of the plasma with respect to the cyclotron instabilities. We have calculated the dispersion  $\omega = \omega(k)$  from Equation (8) in an interval of wave vectors  $0.01 \leq k \leq 2.5$  for the proton and alpha cyclotron branches in a plasma with  $n_\alpha/n_e = 5\%$  (i.e. with the same value as used for Run 4) for a set of proton plasma parameters:  $0.01 \leq \beta_{p\parallel} \leq 30$  and  $1.1 \leq A_p \leq 11$ ; for each of these two parameters we set the parameters of alpha particles to be  $T_{\alpha\parallel} = T_{p\parallel}$  and  $A_\alpha = A_p$ . All species are at the rest,  $v_{e\parallel} = v_{p\parallel} = v_{\alpha\parallel} = 0$  and the electron beta is  $\beta_e = 0.1$ . For each  $\beta_{p\parallel}$  and  $A_p$  and the corresponding parameters of alpha particles we have calculated the maximum growth rate  $\gamma_{AC}$  of the alpha cyclotron instability and of the proton cyclotron one  $\gamma_{PC}$  in the interval of wave vectors. Then we have calculated the maximum growth rate of the two instabilities  $\gamma_{IC} = \max(\gamma_{AC}, \gamma_{PC})$ . The result of this calculation,  $\gamma_{IC} = \gamma_{IC}(\beta_{p\parallel}, A_p)$  with  $T_{\alpha\parallel} = T_{p\parallel}$  and  $A_\alpha = A_p$  is shown in Figure 3 (left panel) as a gray-scale plot (compare with Figure 1). In the right panel of Figure 3 the maximum growth rate  $\gamma_{IC}$  is shown as the gray scale plot, translated to  $\gamma_{IC} = \gamma_{IC}(\beta_{\alpha\parallel}, A_\alpha)$  via the relations  $T_{\alpha\parallel} = T_{p\parallel}$  and  $A_\alpha = A_p$ . Figure 3 (left panel, gray scale plot) clearly exhibits a transition where the proton cyclotron instability dominates,  $\beta_{p\parallel} \lesssim 0.4$ , and where dominates the alpha cyclotron one,  $\beta_{p\parallel} \gtrsim 0.4$ , for moderate growth rates. For strong growth rates it is the proton cyclotron instability that dominates (i.e. for  $\beta_{p\parallel} \gtrsim 1$  and  $A_p \gtrsim 3$ ).

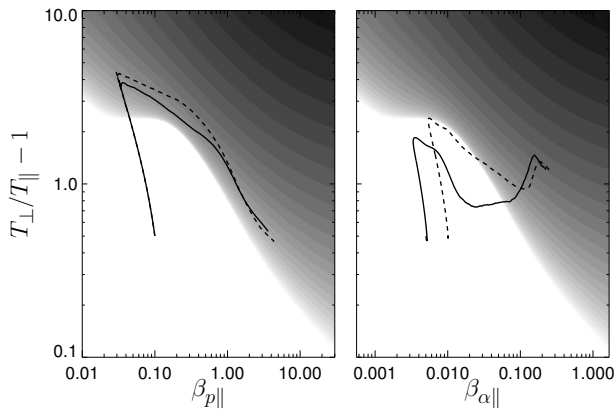


**Figure 3.** Evolution during the plasma compression (left) in the space  $(\beta_{p\parallel}, A_p)$  and (right) in the space  $(\beta_{\alpha\parallel}, A_\alpha)$  for Runs 4 ( $n_\alpha/n_e = 5\%$ , solid curve), and 5 ( $n_\alpha/n_e = 10\%$ , dashed curve); see Table 1. The gray-scale plot denotes the maximum growth rate  $\gamma_{IC}$ .

Results of Runs 4 and 5 are qualitatively similar to the previous results of a pure proton-electron plasma discussed in the previous section. Figure 3 shows that initially, in the stable region the ions follow the CGL prediction, then the system becomes unstable with respect to the proton cyclotron instability and generated waves heat both ion species and overcome the adiabatic forcing. The evolution may not be simply described in terms of  $\gamma_{IC} \sim \text{const}$  even for Run 4. This is, of course, owing to the fact that  $\gamma_{IC}$  was calculated in a two-dimensional subspace of the four-dimensional space

$$(\beta_{p\parallel}, A_p, \beta_{\alpha\parallel}, A_\alpha)$$

setting  $T_{\alpha\parallel} = T_{p\parallel}$  and  $A_\alpha = A_p$ . These relations hold at  $t = 0$  and during the initial adiabatic phase but when the proton cyclotron instability sets on, the generated waves heat preferably alpha particles and the relations are no longer valid. Figure 3 nevertheless shows that the evolutions in Runs 4 and 5 are in a qualitative agreement with predictions of  $\gamma_{IC}$  from the linear theory. The paths in  $(\beta_{p\parallel}, A_p)$  and  $(\beta_{\alpha\parallel}, A_\alpha)$  are not far away from the threshold  $\sim \gamma_{IC} = 0$ , at least for protons, and also for alpha particles in the low-beta region. The behavior of ions, especially of alpha particles (Figure 3, right) is quite complex and needs a detailed examination of the simulation results. From the previous numerical experiments [Hellinger *et al.*, 2003b, and the previous section] we expect that the intensity of the magnetic fluctuation increases with  $\beta_{p\parallel}$  and that in the high-beta plasma the mirror instability appear. From the prediction of the linear theory we also expect an appearance of the alpha cyclotron instability for the high-beta plasma.

Now we focus to the analysis of the evolution of the wave spectra. Figure 4 displays the evolution of the wave energy as a function of  $\beta_{p\parallel}$  (see Figure 3) in Runs 4 and 5: Left panel of Figure 4 shows the total fluctuating wave energy  $|\delta\mathbf{B}|^2/B_0^2$  whereas right panel of Figure 4 shows the correlation  $\langle \delta B_{\parallel}, n_p \rangle$  as a function of  $\beta_{p\parallel}$  for Runs 4 ( $n_\alpha/n_e = 5\%$ , solid curve), and 5 ( $n_\alpha/n_e = 10\%$ , dashed curve); see Table 1.

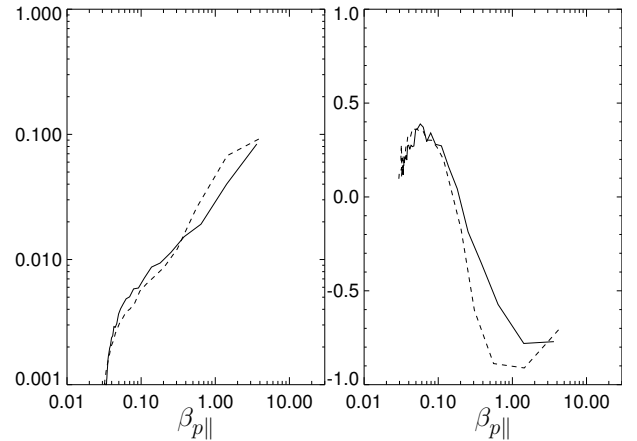


**Figure 4.** (left) The total fluctuating wave energy  $|\delta\mathbf{B}|^2/B_0^2$ , and (right panel) the correlation between  $\delta B_{\parallel}$  and  $n_p$  as a function of  $\beta_{p\parallel}$  for Run 4 ( $n_\alpha/n_e = 5\%$ , solid curve), and 5 ( $n_\alpha/n_e = 10\%$ , dashed curve).

Figure 4 shows that  $|\delta\mathbf{B}|^2/B_0^2$  increases with  $\beta_{p\parallel}$  as expected and that for  $\beta_{p\parallel} \gtrsim 0.3$  the correlation  $\langle \delta B_{\parallel}, n_p \rangle$  becomes negative. This negative value indicates a presence of the mirror mode; the mirror waves are indeed present as we shall see below. Comparison of the results of Runs 4 and 5 with the pure-proton Run 2 (Figure 2) shows that the intensity of fluctuating magnetic field  $|\delta\mathbf{B}|^2/B_0^2$  is in these three simulations at a similar level and that in Runs 4 and 5 the correlation  $\langle \delta B_{\parallel}, n_p \rangle$  becomes negative sooner than in the case of the pure-proton Run 2. The fastest appearance of the anticorrelation is observed in Run 5 ( $n_\alpha/n_e = 10\%$  and  $\beta_{\alpha\parallel 0} = 0.1$ ). These results are in the agreement with the linear theory which predicts that the growth rate of the mirror mode increases when alpha particles are present. Let us now look at the wave properties in detail. Figure 5 displays the spatial wave spectrum  $|\delta\mathbf{B}|^2$  as a function of  $k_{\parallel}$  and  $k_{\perp}$  in Run 4 for four different times with

(left top)  $\beta_{p\parallel} = 0.03$  and  $\beta_{\alpha\parallel} = 0.003$

(right top)  $\beta_{p\parallel} = 0.1$  and  $\beta_{\alpha\parallel} = 0.04$

(left bottom)  $\beta_{p\parallel} = 0.6$  and  $\beta_{\alpha\parallel} = 0.1$

(right bottom)  $\beta_{p\parallel} = 3.6$  and  $\beta_{\alpha\parallel} = 0.2$ .

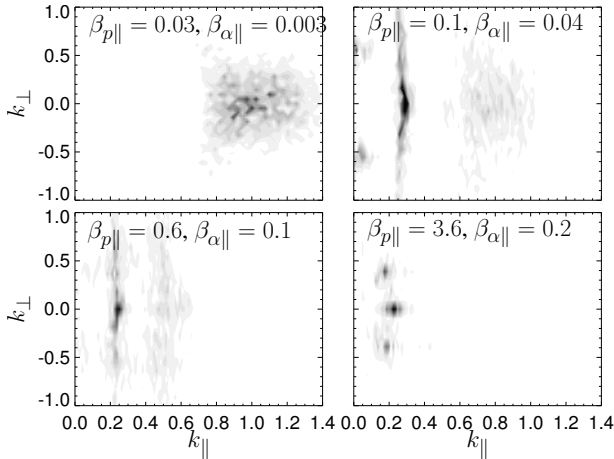


**Figure 5.** Evolution of spectrum in Run 4: The wave spectrum  $|\delta\mathbf{B}|^2$  as a function of  $k_{\parallel}$  and  $k_{\perp}$  for four different  $\beta_{p\parallel}$  and  $\beta_{\alpha\parallel}$ .

Figure 5 demonstrates that the proton cyclotron waves are present initially with large wave vectors  $k_{\parallel} \sim 1$  around the parallel propagation (Figure 5, left top). Soon the alpha cyclotron waves appear for smaller wave vectors  $k_{\parallel} \sim 0.3$  and coexist with the proton cyclotron ones; the mirror waves already appear to be present with nearly perpendicular wave vectors  $k_{\perp} \sim 0.5$ . (Figure 5, right top). The proton cyclotron waves gradually disappear whereas the alpha cyclotron waves become dominant at the parallel propagation with the strong presence of oblique mirror waves (Figure 5, bottom).

### 4.3. Influence of the Alpha/Proton Velocity

In this section we study the question how the plasma behavior changes when the alpha/proton velocity is not zero. First, we note that the CGL prediction of the characteristic plasma velocity, the Alfvén velocity  $v_A$ , varies in the expanding box model. From Equation (6) we have

$$v_A \propto \frac{B}{\sqrt{n}} \propto \frac{1}{\sqrt{1 - \frac{t}{t_c}}}. \quad (12)$$

The CGL predicts that the Alfvén velocity increases with the time whereas the alpha/proton velocity  $v_{\alpha p}$  is constant.

We have performed two Runs 6 and 7 for  $t_c = 2000$  and  $n_{\alpha}/n_e = 5\%$ , with the same initial parameters as we used in the previous section 4.2:  $\beta_{p\parallel 0} = 0.1$ ,  $\beta_{\alpha\parallel 0} = 0.05$  and  $A_{\alpha 0} = A_{p0} = 1.5$ . Moreover, we set the initial alpha/proton velocity to  $v_{\alpha p 0} = 0.5$  for Run 6 and to  $v_{\alpha p 0} = 1$  for Run 7; see Table 1. This choice is stable (as in previous sections 4.1 and 4.2) with respect to both the proton and alpha cyclotron instabilities, and with respect to the mirror one. The system is also stable with respect to the instabilities driven by the alpha/proton velocity [cf. Hellinger *et al.*, 2003a, and references therein].

The evolution of plasma properties during the compression for Runs 6 and 7 is shown in Figure 6 in the same format as in Figures 1 and 3. Figure 6 displays the evolution in the space  $(\beta_{p\parallel}, A_p)$  for Runs 6 ( $v_{\alpha p 0} = 0.5$ , solid curve) and 7 ( $v_{\alpha p 0} = 1$ , dashed curve). As in the previous section we have investigated the growth rate of the ion cyclotron instabilities in a plasma with 5% of alpha particles including the alpha/proton velocity  $v_{\alpha p} = 0.5$ : For each  $\beta_{p\parallel}$  and  $A_p$  and corresponding parameters of alpha particles we have calculated the maximum growth rate  $\gamma_{AC}$  of the alpha cyclotron instability and the maximum growth rate  $\gamma_{PC}$  of the proton cyclotron one in the interval  $0.01 \leq k \leq 2.5$ . Note, that we have investigated both propagations, along and against the alpha/proton velocity  $\mathbf{V}_{\alpha p}$ . From these growth rates we have calculated the maximum

growth rate  $\gamma_{ICd}$  of the two instabilities  $\gamma_{ICd} = \max(\gamma_{AC}, \gamma_{PC})$  for the two propagation directions and for a set of proton parameters:  $0.01 \leq \beta_{p\parallel} \leq 30$  and  $1.1 \leq A_p \leq 11$ . For these proton parameters we set the corresponding parameters of alpha particles to be  $T_{\alpha\parallel} = T_{p\parallel}$  and  $A_{\alpha} = A_p$ . Moreover we set the proton mean velocity to  $v_{p\parallel} = -0.025$  and the mean velocity of alpha particles to  $v_{\alpha\parallel} = 0.225$  so that the alpha/proton velocity is  $v_{\alpha p} = 0.25$ . The electrons have  $v_{e\parallel} = 0$  and  $\beta_e = 0.1$ . The result of this calculation,  $\gamma_{ICd} = \gamma_{ICd}(\beta_{p\parallel}, A_p)$  is shown as a gray-scale plot in Figure 6 (see Figures 1 and 3); darker gray denotes stronger instability whereas white corresponds to stable or marginally stable regions.

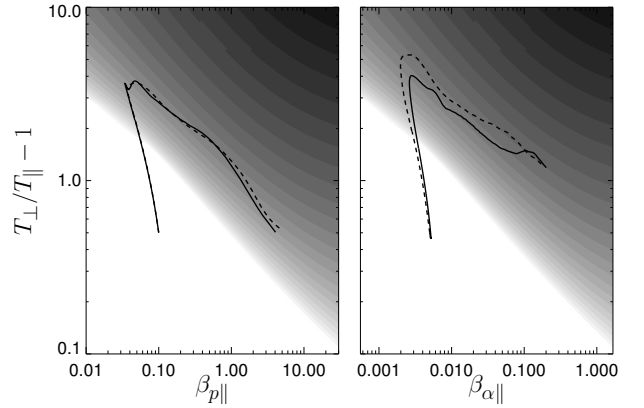


**Figure 6.** Evolution during the plasma compression for (left panel) protons in the space  $(\beta_{p\parallel}, A_p)$  and for (right panel) alpha particles in the space  $(\beta_{\alpha\parallel}, A_{\alpha})$  for Runs 6 ( $v_{\alpha p 0} = 0.5$ , solid curve) and 7 ( $v_{\alpha p 0} = 1$ , dashed curve); see Table 1. The gray-scale plot denotes the maximum growth rate  $\gamma_{ICd}$ .

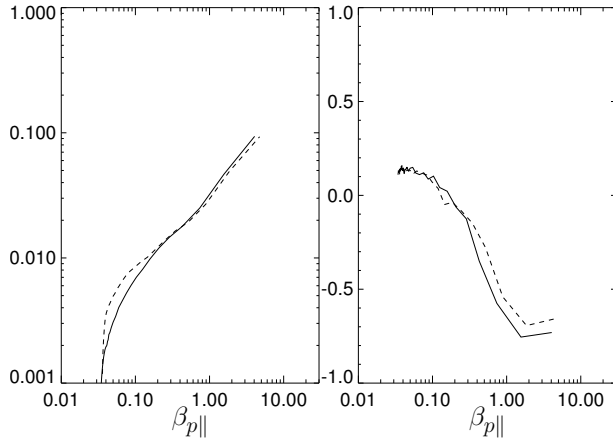
The results of Runs 6 and 7 are qualitatively similar to the previous results of the pure proton-electron plasma (Run 2) and the plasma with the small abundance of alpha particles but without the alpha/proton velocity (Runs 4 and 5). Figure 6 shows that initially, in the stable region the ions follow the CGL prediction, then the system becomes unstable with respect to the proton cyclotron instability and generated waves heat both ion species and overcome the adiabatic forcing. The evolution may not be simply described in terms of  $\gamma_{ICd} \sim \text{const}$  even for Run 6 for the same reason as in the previous section:  $\gamma_{IC}$  was calculated in a two-dimensional subspace of the five-dimensional space

$$(\beta_{p\parallel}, A_p, \beta_{\alpha\parallel}, A_{\alpha}, v_{\alpha p})$$

setting  $T_{\alpha\parallel} = T_{p\parallel}$ ,  $A_{\alpha} = A_p$  and  $v_{\alpha p} = 0.5$ . These relations hold only at  $t = 0$ ;  $v_{\alpha p}/v_A$  decreases even during the initial adiabatic phase. Generated waves heat and accelerate alpha particles and the adiabatic behavior is strongly broken when the proton cyclotron instability sets on. As in the previous section the linear prediction is relatively robust. Figure 6 shows that the evolutions in Runs 6 and 7 are close to each other and are in a qualitative agreement with the predictions of  $\gamma_{ICd}$ . The paths in  $(\beta_{p\parallel}, A_p)$  and  $(\beta_{\alpha\parallel}, A_{\alpha})$  are not far away from the threshold  $\sim \gamma_{ICd} = 0$ . The behavior of protons and alpha particles (Figure 6) is much less complex than in the previous section, especially for alpha particles (Figure 3, right). The proton evolution (Figures 6, left) is similar to the pure proton-electron plasma of Run 2 (Figures 1). The streaming alpha particles do not change the plasma behavior so drastically as the alpha particles with no relative velocity with respect to the protons.

Let us now examine the simulation results in detail and compare them with the results of the previous section. Figure 7 displays the evolution of the wave spectrum (see Figure 6) in Runs 6

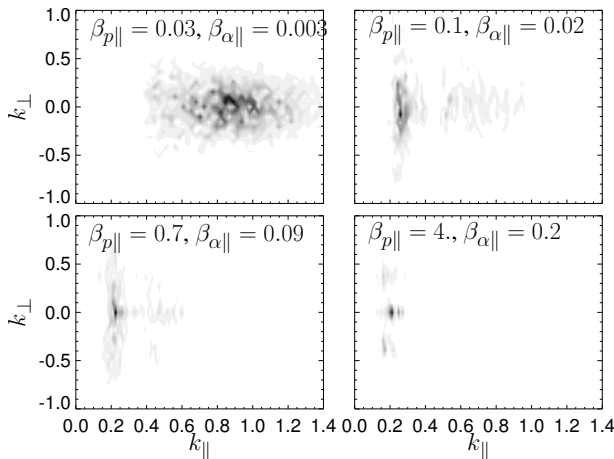
( $v_{\alpha p0} = 0.5$ , solid curve) and 9 ( $v_{\alpha p0} = 1$ , dashed curve): Left panel of Figure 7 shows the total fluctuating wave energy  $|\delta\mathbf{B}|^2/B_0^2$  whereas right panel of Figure 4 shows the correlation between  $\delta B_{\parallel}$  and  $n_p$  as a function of  $\beta_{p\parallel}$ .



**Figure 7.** (left panel) The total fluctuating wave energy  $|\delta\mathbf{B}|^2/B_0^2$ , and (right panel) the correlation  $\langle \delta B_{\parallel}, n_p \rangle$  as a function of  $\beta_{p\parallel}$  for Run 6 ( $v_{\alpha p0} = 0.5$ , solid curve) and 7 ( $v_{\alpha p0} = 1$ , dashed curve).

Figure 8 shows the evolution of wave spectrum in Run 6: The spatial wave spectrum  $|\delta\mathbf{B}|^2$  as a function of  $k_{\parallel}$  and  $k_{\perp}$  for four different times of the simulations with:

- (left top)  $\beta_{p\parallel} = 0.03$  and  $\beta_{\alpha\parallel} = 0.003$ ,
- (right top)  $\beta_{p\parallel} = 0.1$  and  $\beta_{\alpha\parallel} = 0.02$ ,
- (left bottom)  $\beta_{p\parallel} = 0.7$  and  $\beta_{\alpha\parallel} = 0.09$ , and
- (right bottom)  $\beta_{p\parallel} = 4$  and  $\beta_{\alpha\parallel} = 0.2$ .



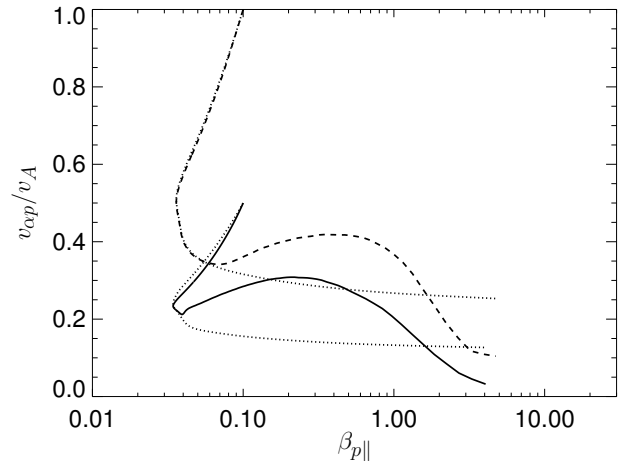
**Figure 8.** Evolution of spectrum in Run 6: Spatial wave spectrum  $|\delta\mathbf{B}|^2$  as a function of  $k_{\parallel}$  and  $k_{\perp}$  for four different  $\beta_{p\parallel}$  and  $\beta_{\alpha\parallel}$ .

Figure 8 shows that initially the proton cyclotron waves are present with large wave vectors  $k_{\parallel} \sim 0.8$  around the parallel propagation (Figure 8, left top). Soon the alpha cyclotron waves appear for smaller wave vectors  $k_{\parallel} \sim 0.3$  and coexist with the proton cyclotron ones. The proton cyclotron waves gradually disappear whereas the alpha cyclotron waves become dominant at the parallel propagation (Figure 8, left bottom). Later on, in the high-beta plasma, a mirror mode appears with oblique wave vectors (Fig-

ure 8, right bottom). The simulation result of Run 6 are similar to the results of Run 4 without the alpha/proton velocity. One notable aspect of Run 6 is that the mirror waves appear in higher beta region in Run 6 comparing with Run 4. The alpha/proton velocity lower the growth rate of the mirror instability since the parallel ion velocities contribute to the effective parallel temperature, lowering the effective temperature anisotropy for the nonresonant mirror instability.

The comparison of Figures 3 for Run 4 and Figure 6 suggests that the important heating of alpha particles in Run 4 is due to the mirror waves. The non-propagating mirror waves may interact with slowly or not propagating alpha particles of Run 4 in an efficient way. On the other hand, the alpha particles streaming with non negligible velocity with respect to the mirror waves should be slowed down; this is one of the possible mechanisms for the alpha deceleration in the high-beta simulations of *Gary et al.* [2003].

Let us examine the alpha/proton velocity evolution Runs 6 and 7. Figure 9 shows the evolution of the ratio between the alpha/proton velocity and the Alfvén velocity  $v_{\alpha p}/v_A$  as a function of  $\beta_{p\parallel}$  for Runs 6 ( $v_{\alpha p0} = 0.5$ , solid curve) and 7 ( $v_{\alpha p0} = 1$ , dashed curve). The CGL prediction (Equation (12)) of the ratio  $v_{\alpha p}/v_A$  is denoted by two dotted curves, one for each simulation.



**Figure 9.** Evolution in Runs 6 ( $v_{\alpha p0} = 0.5$ , solid curve) and 7 ( $v_{\alpha p0} = 1$ , dashed curve) of the ratio  $v_{\alpha p}/v_A$  as a function of  $\beta_{p\parallel}$ . The dotted curves shows the CGL predictions.

Figure 9 shows that initially, in the stable region the ions follow the CGL predictions (compare with Figure 6). Then the system becomes unstable with respect to the proton cyclotron instability and generated waves accelerate alpha particles with respect to protons. The acceleration is stopped when the alpha cyclotron waves appear and the alpha particles are slowed down. The role of the mirror waves which appear in the high-beta plasma is difficult to discern. In order to do this, we have performed a classical 2-D hybrid simulation with the initial parameters similar to those used by *Gary et al.* [2003]. In the simulation the proton cyclotron waves try to accelerate the alpha particles whereas the mirror waves decelerate them as we expected.

## 5. Discussion

In this paper we have extended the work of *Hellinger et al.* [2003b] on the effects of a slow compression on the plasma properties. We have shown that under condition of a slow compression the plasma system follows the marginal stability path of the proton cyclotron instability in low-beta region. This path depends on the characteristic compression time: In a proton-electron plasma this path may be given as

$$\gamma(\beta_{p\parallel}, A_p) \sim \gamma_{\text{marg}} = \text{const.}, \quad (13)$$

where  $\gamma(\beta_{p\parallel}, A_p)$  is the maximum growth rate of the proton cyclotron instability in a pure electron-proton plasma with bi-Maxwellian protons characterized by  $\beta_{p\parallel}$  and  $A_p$ . The  $\gamma_{\text{marg}}$  is inversely proportional to the characteristic compression time

$$\gamma_{\text{marg}} \propto \frac{1}{t_c}. \quad (14)$$

For a stronger compression (smaller  $t_c$ ) the marginal stability path is characterized by a stronger instability  $\gamma_{\text{marg}}$  and a stronger ion cyclotron turbulence (see Figure 2). The constant growth-rate behavior of Equation (13) is disrupted in high beta plasma owing to the appearance of mirror waves [cf. *Hellinger et al.*, 2003b].

It is interesting to discuss the anticorrelation of Equation (14) with results of *Pudovkin et al.* [2002a], *Pudovkin et al.* [2002a] analyzed variations of the proton temperature anisotropy  $A_p$  and the plasma wave turbulence characteristics across the magnetosheath and compared these observations with predictions of the bounded anisotropy model based on the marginal stability condition. *Pudovkin et al.* [2002a] showed that the deviation of the observed values of  $A_p$  from the bounded anisotropy model (the marginal stability) may be explained by a finite value of the temperature isotropization time  $\tau$ . The estimated values of  $\tau$  have a tendency to be anticorrelated with the intensity of the magnetic field oscillations. In our simulations the compression is balanced by the waves so that characteristic time  $t_c$  is related to the isotropization time  $\tau$ . If we assume that  $\tau \propto t_c$  we recover the anticorrelation observed by *Pudovkin et al.* [2002a] between  $\tau$  and the amplitude of the magnetic field oscillations. In the high-beta region where the mirror mode appears this behavior becomes more complicated; for the slowest compression time  $t_c = 4000$  the mirror mode grows faster than in the case of  $t_c = 2000$ , probably because has more time to develop. This phenomenon and the properties of the mirror mode are in general important problem [cf. *Hill et al.*, 1995; *Pudovkin et al.*, 2002a], however further studies in this direction are beyond the scope of this paper.

The presence of alpha particles changes properties of the plasma during the compression, as it is expected from the prediction of the linear theory [*Gary et al.*, 1993b; *Gratton and Farrugia*, 1996; *Gnavi et al.*, 2000]. Two ion cyclotron instabilities, the proton and alpha ones, and the mirror instability may become unstable for proton and/or alpha particles temperature anisotropy  $T_{\perp} > T_{\parallel}$ . The proton cyclotron instability is dominant in low-beta, low-alpha-particle abundance whereas the alpha cyclotron instability is important in a high-beta, high alpha-particle temperature anisotropy and abundance. The mirror mode also becomes more important with the presence of alpha particles. The HEB simulations confirm these theoretical predictions. The slowly compressed plasma with protons and alpha particles follows the marginal stability path; initially in low-beta plasma this path is determined by the proton cyclotron instability, in higher-beta plasma the alpha cyclotron waves appear and continually replace the proton cyclotron waves and finally in even higher beta plasma the mirror waves appear and coexist with the alpha cyclotron waves. The marginal stability path is more complicated than that in the pure electron-proton plasma but the difference is not big. The simulation results are close to the marginal stability predictions based on the linear prediction  $\gamma(\beta_{p\parallel}, A_p)$ , calculated for the anisotropic, pure electron-proton plasma.

A nonzero alpha/proton relative velocity makes the theoretical understanding of the linear properties of the plasma even more complicated [*Gary et al.*, 2003]. The alpha/proton velocity is another free parameter that changes the plasma properties and influences instabilities controlling the ion thermodynamics of magnetosheath compression. The HEB simulations show the streaming alpha particles do not change so drastically the plasma behavior as the alpha particles with no relative velocity with respect to the protons. The qualitative behavior of the compressed system with the nonzero alpha/proton velocity is similar to the behavior of the system without the alpha/proton velocity. The slowly compressed

plasma follows the marginal stability path; initially in low-beta plasma this path is determined by the proton cyclotron instability, in higher-beta plasma the alpha cyclotron waves appear and continually replace the proton cyclotron waves and finally in even higher beta plasma the mirror waves appear and coexist with the alpha cyclotron waves. The nonzero alpha/proton velocity lower the growth rate of the mirror instability since the parallel ion velocities contribute to the effective parallel temperature, lowering the effective temperature anisotropy for the nonresonant mirror instability. The compressed system of the nonzero alpha/proton velocity case reveal a new feature. During the first, the proton cyclotron phase, the alpha particles are efficiently accelerated with respect to protons in agreement with the hypothesis of heating and acceleration of the solar wind by cyclotron waves [cf. *Gomberoff et al.*, 1996]. The result is also in agreement with quasi-linear expectations and the quasi-linear phase of the simulations by *Gary et al.* [2003]. When the alpha cyclotron waves appear they decelerate the alpha particles [in agreement with results of *Gary et al.*, 2003]. The appearance of the mirror waves also leads to the deceleration of alpha particles. The mirror mode which becomes important in the high beta plasma is probably responsible for the strong deceleration of the alpha particles in the simulations by *Gary et al.* [2003]; the role of ion cyclotron and mirror instabilities in the solar wind context should be revisited.

## 6. Conclusion

We have investigated the effect of the slow compression on the plasma and the role of characteristic compression time, alpha particles and alpha/proton speed. Presented results are relevant for the magnetosheath regions dominated by compression [cf. *Lucek et al.*, 1999]. During the compression waves are continuously generated and keep the system near the marginal stability. The marginal stability evolution is close to the linear predictions based on the pure electron-proton plasma dispersion relation [cf. *Fuselier et al.*, 1994; *Gary et al.*, 1994c] even in the system with alpha particles; this prediction is quite robust in agreement with observations. However, the presence of alpha particles bring some nonnegligible variations. The nonzero alpha/proton velocity, a possible remnant from the fast solar wind and/or a consequence of the different deceleration of alpha particles and protons in the shock [*Peterson et al.*, 1979; *Zhao et al.*, 1991], also appear to change the plasma properties, bringing them back closer to the pure electron-proton plasma. It is noteworthy that the proton cyclotron waves are able to efficiently accelerate the alpha particles with respect to the protons (Runs 6 and 7).

The compression is only one of the macroscopic processes in the magnetosheath. The magnetosheath plasma flow around the magnetospheric cavity leads also to the expansion (especially to the field-line stretching) and to the velocity shears. All these processes (along with the compression) are usually at work simultaneously and influence the microscopic plasma properties. These phenomena and their combinations will be subject of future works.

## Appendix: Expanding Box Model

Let us derive the Vlasov equation for the expanding box model: In a given Cartesian frame  $\mathbf{x}$  the Vlasov equation has the usual form

$$\frac{\partial f}{\partial t} + \mathbf{v} \cdot \frac{\partial f}{\partial \mathbf{x}} + \frac{q}{m} (\mathbf{E} + \mathbf{v} \times \mathbf{B}) \cdot \frac{\partial f}{\partial \mathbf{v}} = 0. \quad (A1)$$

We suppose an external force make the mean plasma flow to evolve as  $\mathbf{x}(t) = \mathbf{L}(t) \cdot \mathbf{x}(0)$  where  $\mathbf{L}$  is a diagonal matrix  $\mathbf{L}(t) = \text{diag}(L_x, L_y, L_z)$  with  $\mathbf{L}(0) = \mathbf{1}$ ,  $d\mathbf{L}/dt = \text{diag}(dL_x/dt, dL_y/dt, dL_z/dt)$ , and  $d^2\mathbf{L}/dt^2 = 0$ .  $\mathbf{1}$  denotes the unity matrix. The mean velocity  $\mathbf{U}$  may be given as

$$\mathbf{U}(\mathbf{x}(t)) = \frac{d\mathbf{x}}{dt} = \mathbf{V} \cdot \mathbf{x}(t)$$

where  $\mathbf{V} = \mathbf{L}^{-1} \cdot d\mathbf{L}/dt$ ,  $\mathbf{L}^{-1}$  being the inverse matrix of  $\mathbf{L}$ . If we now change the frame  $t = t$ ,  $\tilde{\mathbf{x}} = \mathbf{x}$ , and  $\tilde{\mathbf{v}} = \mathbf{v} - \mathbf{U}$  (non-Galilean transformation) we have

$$\frac{\partial f}{\partial t} + (\tilde{\mathbf{v}} + \mathbf{U}) \cdot \frac{\partial f}{\partial \tilde{\mathbf{x}}} - \tilde{\mathbf{v}} \cdot \frac{\partial \mathbf{U}}{\partial \tilde{\mathbf{x}}} \cdot \frac{\partial f}{\partial \tilde{\mathbf{v}}} + \frac{q}{m} (\tilde{\mathbf{E}} + \tilde{\mathbf{v}} \times \mathbf{B}) \cdot \frac{\partial f}{\partial \tilde{\mathbf{v}}} = 0 \quad (A2)$$

where  $\tilde{\mathbf{E}} = \mathbf{E} + \mathbf{U} \times \mathbf{B}$ . If we now change to the co-moving coordinates  $\boldsymbol{\xi} = \mathbf{L}^{-1} \cdot \tilde{\mathbf{x}}$ ,  $t = \tilde{t}$ , and  $\boldsymbol{\nu} = d\boldsymbol{\xi}/d\tilde{t}$  we have

$$\frac{\partial f}{\partial t} + \boldsymbol{\nu} \cdot \frac{\partial f}{\partial \boldsymbol{\xi}} + \frac{q}{m} (\tilde{\mathbf{E}} + (\mathbf{L} \cdot \boldsymbol{\nu}) \times \mathbf{B}) \cdot \mathbf{L}^{-1} \cdot \frac{\partial f}{\partial \boldsymbol{\nu}} = 2\boldsymbol{\nu} \cdot \mathbf{V} \cdot \frac{\partial f}{\partial \boldsymbol{\nu}}. \quad (\text{A3})$$

Equation (A3) in the co-moving coordinates has a structure similar to the Vlasov equation (A1). Similarly we may calculate the modification of the equation

$$\frac{\partial \mathbf{B}}{\partial t} = -\frac{\partial}{\partial \mathbf{x}} \times \mathbf{E} \quad (\text{A4})$$

in the co-moving coordinates. It turns to have the following form:

$$\frac{\partial \mathbf{B}}{\partial t} = \{\mathbf{V} - \text{tr}(\mathbf{V})\mathbf{1}\} \cdot \mathbf{B} - \left( \mathbf{L}^{-1} \cdot \frac{\partial}{\partial \boldsymbol{\xi}} \right) \times \tilde{\mathbf{E}} \quad (\text{A5})$$

where  $\text{tr}$  denotes trace of a matrix. If we denote  $l$  the determinant of  $\mathbf{L}$ ,  $l = \det \mathbf{L}$  and if we define modified magnetic and electric fields as

$$\mathbf{B} = l\mathbf{L}^{-1} \cdot \tilde{\mathbf{B}}, \quad \mathcal{E} = \mathbf{L} \cdot \tilde{\mathbf{E}} \quad (\text{A6})$$

then Equation (A5) obtains the following form:

$$\frac{\partial \mathbf{B}}{\partial t} = -\frac{\partial}{\partial \boldsymbol{\xi}} \times \mathcal{E} \quad (\text{A7})$$

and the Vlasov equation (A3) then reads

$$\frac{\partial f}{\partial t} + \boldsymbol{\nu} \cdot \frac{\partial f}{\partial \boldsymbol{\xi}} + \frac{q}{m} (\mathcal{E} + \boldsymbol{\nu} \times \mathbf{B}) \cdot \mathbf{L}^{-2} \cdot \frac{\partial f}{\partial \boldsymbol{\nu}} = 2\boldsymbol{\nu} \cdot \mathbf{V} \cdot \frac{\partial f}{\partial \boldsymbol{\nu}}. \quad (\text{A8})$$

From the generalized Ohm's law [Matthews, 1994]

$$\tilde{\mathbf{E}} = -\frac{\mathbf{J}_p \times \mathbf{B}}{en} - \frac{\text{grad} p_e}{en} + \frac{(\text{rot} \mathbf{B}) \times \mathbf{B}}{e\mu_0 n} \quad (\text{A9})$$

we have an equation for  $\mathcal{E}$  in the following form

$$\mathcal{E} = -\frac{\mathcal{J} \times \mathbf{B}}{e\mathcal{N}} - \frac{l}{e\mathcal{N}} \frac{\partial p_e}{\partial \boldsymbol{\xi}} + \left( \frac{\partial}{\partial \boldsymbol{\xi}} \times \mathbf{B} \right) \times \frac{\mathbf{L}^2 \mathbf{B}}{e\mu_0 l \mathcal{N}} \quad (\text{A10})$$

where  $\mathcal{N} = 1/e \sum q \int f(\boldsymbol{\xi}, \boldsymbol{\nu}) d^3 \boldsymbol{\nu}$  and  $\mathcal{J} = \sum q \int \boldsymbol{\nu} f(\boldsymbol{\xi}, \boldsymbol{\nu}) d^3 \boldsymbol{\nu}$  (summing goes over all the ion species) are related to the physical density  $n$  and the ion current  $\mathbf{J}$  as  $n = \mathcal{N}/l$  and  $\mathbf{J}/l$ , respectively. To close the system we suppose that electrons are isothermal,  $p_e = nk_B T_e$ , where  $k_B$  is Boltzmann constant and  $T_e$  is constant.

**Acknowledgments.** Authors thank Catherine Lacombe and André Mangeney for useful discussions and acknowledge grants GA CR 205/01/P079, GA AV IAA3042403 and ESA PRODEX contract No. 14529/00/NL/SFe(IC).

## References

- Anderson, B. J., and S. A. Fuselier (1993), Magnetic pulsations from 0.1 to 4 hz and associated plasma properties in the Earth's subsolar magnetosheath and plasma depletion layer, *J. Geophys. Res.*, *98*, 1461–1479.
- Anderson, B. J., S. A. Fuselier, S. P. Gary, and R. E. Denton (1994), Magnetic spectral signatures in the Earth's magnetosheath and plasma depletion layer, *J. Geophys. Res.*, *99*, 5877–5891.
- Bame, S. J., J. R. Asbridge, W. C. Feldman, and M. D. Montgomery (1975), Solar wind heavy ion abundances, *Solar Phys.*, *43*, 463–473.
- Belmont, G., and C. Mazelle (1992), Polytopic indices in collisionless plasmas: Theory and mesuments, *J. Geophys. Res.*, *97*, 8327–8336.
- Chew, G. F., M. L. Goldberger, and F. E. Low (1956), The Boltzmann equation and the one fluid hydromagnetic equations in the absence of particle collisions, *Proc. R. Soc. London*, *A236*, 112–118.
- Denton, R. E., B. J. Anderson, S. P. Gary, and S. A. Fuselier (1994), Bounded anisotropy fluid model for ion temperatures, *J. Geophys. Res.*, *99*, 11,225–11,241.

- Erkaev, N. V., H. K. Biernat, and C. J. Farrugia (2000), Ideal magnetohydrodynamic flow around a blunt body under anisotropic pressure, *Phys. Plasmas*, *7*, 3413–3420.
- Farrugia, C. J., N. V. Erkaev, D. F. Vogl, H. K. Biernat, M. Oieroset, R. P. Lin, and R. P. Lepping (2001), Anisotropic magnetosheath: Comparison of theory with Wind observations near the stagnation streamline, *J. Geophys. Res.*, *106*, 29,373–29,385.
- Fuselier, S. A., E. G. Shelley, and D. M. Klumppar (1988), AMPTE/CCE observations of shell-like  $\text{He}^{2+}$  and  $\text{O}^{6+}$  distributions in the magnetosheath, *Geophys. Res. Lett.*, *15*, 1333–1336.
- Fuselier, S. A., B. J. Anderson, S. P. Gary, and R. E. Denton (1994), Inverse correlations between the ion temperature anisotropy and plasma-beta in the Earth's quasi-parallel magnetosheath, *J. Geophys. Res.*, *99*, 14,931–14,936.
- Gary, S. P., S. A. Fuselier, and B. J. Anderson (1993a), Ion anisotropy instabilities in the magnetosheath, *J. Geophys. Res.*, *98*, 1481–1488.
- Gary, S. P., M. E. McKean, and D. Winske (1993b), Ion-cyclotron anisotropy instabilities in the magnetosheath – theory and simulations, *J. Geophys. Res.*, *98*, 3963–3971.
- Gary, S. P., B. J. Anderson, R. E. Denton, S. A. Fuselier, and M. E. McKean (1994a), A limited closure relation for anisotropic plasmas from the Earth's magnetosheath, *Phys. Plasmas*, *1*, 1676–1683.
- Gary, S. P., P. D. Convery, R. E. Denton, S. A. Fuselier, and B. J. Anderson (1994b), Proton and helium cyclotron anisotropy thresholds in the magnetosheath, *J. Geophys. Res.*, *99*, 5915–5921.
- Gary, S. P., M. E. McKean, D. Winske, B. J. Anderson, R. E. Denton, and S. A. Fuselier (1994c), The proton cyclotron instability and the anisotropy/beta inverse correlation, *J. Geophys. Res.*, *99*, 5903–5914.
- Gary, S. P., L. Yin, and D. Winske (2000), Electromagnetic proton cyclotron anisotropy instability: Wave-particle scattering rate, *Geophys. Res. Lett.*, *27*, 2457–2459.
- Gary, S. P., L. Yin, D. Winske, L. Ofman, B. E. Goldstein, and M. Neugebauer (2003), Consequences of proton and alpha anisotropies in the solar wind: Hybrid simulations, *J. Geophys. Res.*, *108*, 1068, doi: 10.1029/2002JA009654.
- Gnavi, G., F. T. Gratton, and C. J. Farrugia (2000), Theoretical properties of electromagnetic ion cyclotron waves in the terrestrial, dayside, low-latitude plasma depletion layer under uncompressed magnetosheath conditions, *J. Geophys. Res.*, *105*, 20,973–20,988.
- Gomberoff, L., F. T. Gratton, and G. Gnavi (1996), Acceleration and heating of heavy ions by circularly polarized Alfvén waves, *J. Geophys. Res.*, *101*, 15,661–15,666.
- Gratton, F. T., and C. J. Farrugia (1996), Electromagnetic ion cyclotron waves in the terrestrial plasma depletion layer: Effects of possible differential speeds between thermal  $\text{H}^+$  and  $\text{He}^{2+}$  ions, *J. Geophys. Res.*, *101*, 21,553–21,560.
- Hau, L. N. (1996), Nonideal MHD effects in the magnetosheath, *J. Geophys. Res.*, *101*, 2655–2660.
- Hellinger, P., P. Trávníček, A. Mangeney, and R. Grappin (2003a), Hybrid simulations of the expanding solar wind: Temperatures and drift velocities, *Geophys. Res. Lett.*, *30*, 1211, doi:10.1029/2002GL016409.
- Hellinger, P., P. Trávníček, A. Mangeney, and R. Grappin (2003b), Hybrid simulations of the magnetosheath compression: Marginal stability path, *Geophys. Res. Lett.*, *30*, 1959, doi:10.1029/2003GL017855.
- Hill, P., G. Paschmann, R. A. Treumann, W. Baumjohann, and H. Lühr (1995), Plasma and magnetic field behavior across the magnetosheath near local noon, *J. Geophys. Res.*, *100*, 9575–9583.
- Hubert, D., C. Lacombe, C. C. Harvey, M. Moncuquet, C. T. Russell, and M. F. Thomsen (1998), Nature, properties, and origin of low-frequency waves from an oblique shock to the inner magnetosheath, *J. Geophys. Res.*, *103*, 26,783–26,798.
- Lacombe, C., and G. Belmont (1995), Waves in the Earth's magnetosheath: Observations and interpretations, *Adv. Space Res.*, *15*, 329–340.
- Li, X., and S. R. Habbal (2000), Proton/alpha magnetosonic instability in the fast solar wind, *J. Geophys. Res.*, *105*, 7483–7489.
- Liewer, P. C., M. Velli, and B. E. Goldstein (2001), Alfvén wave propagation and ion cyclotron interaction in the expanding solar wind: One-dimensional hybrid simulations, *J. Geophys. Res.*, *106*, 29,261–29,281.
- Lucek, E. A., M. W. Dunlop, A. Balogh, P. J. Cargill, W. Baumjohann, E. Georgescu, G. Haerendel, and K.-H. Fornacon (1999), Identification of magnetosheath mirror modes in Equator-S magnetic field data, *Ann. Geophys.*, *17*, 1560–1573.
- Manheimer, W., and J. P. Boris (1977), Marginal stability analysis: A simpler approach to anomalous transport in plasmas, *Comments Plasma Phys. Controlled Fusion*, *3*, 15–24.
- Marsch, E., K. H. Muhlhäuser, H. Rosenbauer, R. Schwenn, and F. M. Neubauer (1982), Solar-wind helium ions – observations of the Helios solar probes between 0.3-AU and 1-AU, *J. Geophys. Res.*, *87*, 35–51.

- Matsuoka, A., D. J. Southwood, T. Mukai, S. Kokubun, and H. Matsumoto (2002), A Walén test of low-frequency MHD waves in the magnetosheath observed by geotail, *Planet. Space Sci.*, *50*, 613–618.
- Matthews, A. (1994), Current advance method and cyclic leapfrog for 2D multispecies hybrid plasma simulations, *J. Comput. Phys.*, *112*, 102–116.
- McKean, M. E., D. Winske, and S. P. Gary (1994), 2-dimensional simulations of ion anisotropy instabilities in the magnetosheath, *J. Geophys. Res.*, *99*, 11,141–11,153.
- Neugebauer, M., B. E. Goldstein, E. J. Smith, and W. C. Feldman (1996), Ulysses observations of differential alpha-proton streaming in the solar wind, *J. Geophys. Res.*, *101*, 17,047–17,056.
- Ogilvie, K. W., M. A. Coplan, and R. D. Zwickl (1982), Helium, hydrogen, and oxygen velocities observed on ISEE 3, *J. Geophys. Res.*, *87*, 7363–7369.
- Peterson, W. K., E. G. Shelley, R. D. Sharp, R. G. Johnson, J. Geiss, and H. Rosenbauer (1979),  $H^+$  and  $He^{2+}$  in the dawnside magnetosheath, *Geophys. Res. Lett.*, *6*, 667–670.
- Phan, T. D., G. Paschmann, W. Baumjohann, N. Sckopke, and H. Lühr (1994), The magnetosheath region adjacent to the dayside magnetopause – AMPTE/IRM observations, *J. Geophys. Res.*, *98*, 121–141.
- Pudovkin, M. I., S. A. Zaitseva, B. P. Besser, W. Baumjohann, C. V. Meister, and A. L. Maulini (2002a), Proton pitch angle diffusion rate and wave turbulence characteristics in the magnetosheath plasma, *J. Geophys. Res.*, *107*, 1402, doi:10.1029/2001JA009149.
- Pudovkin, M. I., S. A. Zaitseva, V. V. Lebedeva, A. A. Samsonov, B. P. Besser, C.-V. Meister, and W. Baumjohann (2002b), MHD-modelling of the magnetosheath, *Planet. Space Sci.*, *50*, 473–488.
- Reisenfeld, D. B., S. P. Gary, J. T. Gosling, J. T. Steinberg, D. J. McComas, B. E. Goldstein, and M. Neugebauer (2001), Helium energetics in the high-latitude solar wind: Ulysses observations, *J. Geophys. Res.*, *106*, 5693–5708.
- Schwartz, S. J., D. Burgess, and J. J. Moses (1996), Low-frequency waves in the Earth's magnetosheath: Present status, *Ann. Geophys.*, *14*, 1134–1150.
- Stix, T. H. (1992), *Waves in plasmas*, AIP, New York.
- Zhao, X., K. W. Ogilvie, and Y. C. Whang (1991), Modeling the effects of fast shocks on solar winds ions, *J. Geophys. Res.*, *96*, 5437–5445.

---

P. Hellinger and P. Trávníček, Institute of Atmospheric Physics, AS CR, Prague 14131, Czech Republic. (Petr.Hellinger@ufa.cas.cz; trav@ufa.cas.cz)